Journal of Solid State Chemistry 184 (2011) 790–796

Contents lists available at ScienceDirect

Journal of Solid State Chemistry

journal homepage: www.elsevier.com/locate/jssc

HRTEM and neutron diffraction study of $Li_xMo_5O_{17}$: From the ribbon ($x=5$) structure to the rock salt ($x=12$) structure

O.I. Lebedev [a], V. Caignaert [a], B. Raveau [a], N. Pop [a], F. Gozzo [b], G. Van Tendeloo [c], V. Pralong [a,*]

[a] Laboratoire CRISMAT, CNRS ENSICAEN, Universite Caen, 6 bd Maréchal Juin, 14050 Caen, France
[b] PSI Laboratoire, Swiss Light Source, CH-5232 Villigen, Switzerland
[c] EMAT, University of Antwerpen, Groenenborgerlaan 171, B2020 Antwerpen, Belgium

ARTICLE INFO

Article history:
Received 28 September 2010
Received in revised form
12 January 2011
Accepted 2 February 2011
Available online 24 February 2011

Keywords:
Li intercalation
Molybdenum oxide
HRTEM
Neutron

ABSTRACT

Structure determination of the fully intercalated phase $Li_{12}Mo_5O_{17}$ and of the deintercalated oxide $Li_5Mo_5O_{17}$ has been carried out by electron microscopy and neutron powder diffraction. The reversible topotactic transformation between the ordered rock salt structure of the former and the ribbon structure of the latter (closely related to that of $Li_4Mo_5O_{17}$) is explained on the following basis: both structures can be described as strips built up as an assembly of infinite ribbons of MoO_6 octahedra that are five octahedra thick, and that differ by slight displacements of the octahedral ribbons. We show that the electrochemical behavior of the $Li_xMo_5O_{17}$ system is based on two sorts of Li^+ sites; those that are located within the strips between the ribbons, and those that are located at the border of the strips. The high rate of Li intercalation in this oxide and its reversibility are discussed in terms of its peculiar structure.

1. Introduction

Numerous transition metal oxides such as those based on cobalt, manganese, nickel, vanadium, tungsten, titanium, niobium or molybdenum, are of great interest for lithium insertion in view of the realization of Li-ion batteries [1–6], because of the adequate value of the redox potential of the transition element. Molybdenum oxides have been investigated previously also because of their benign environmental behavior. Note therefore that the redox potential values for the couples Mo^{6+}/Mo^{5+} is 2.4 V and for the couples Mo^{5+}/Mo^{4+} is about 1.6 V. This is the case for the Mo(VI) oxide MoO_3 which was studied as a cathode material [7–12] and for the Mo (IV) oxides Li_2MoO_3 [13–15] and $Li_4Mo_5O_{12}$ [13] which were found to exhibit capacity values of 150 and 123 mA h/g, respectively, whereas the bronze Li_xMoO_3 [9] was shown to be an interesting anode material with a retention capacity of 600 mA h/g after 100 cycles.

Considering the structure of several lithium molybdates [16–19], the possibility of lithium intercalation in one of them, $Li_4Mo_5O_{17}$, was recently investigated [20], on the basis of its ribbon structure. It was shown that this oxide can intercalate up to eight lithium ions per formula, according to a reversible topotactic reaction, leading to an ordered rock salt structure. Note that such an intercalation reaction leading to a rock salt structure, though it has been often observed in other oxides [21], involves an exceptionally high amount of lithium i.e. 1.6 Li per Mo.

However, the large number of positional parameters (102 for 34 independent atoms) and the small atomic number of lithium in the end member $Li_{12}Mo_5O_{17}$, did not allow us to locate and refine the positions of the Li^+ cations from the XRPD data. The latter could only be deduced from the bond valence sum calculations and consequently these hypothetic positions have to be verified. In the present study, we have explored the fully Li-intercalated member using high resolution transmission electron microscopy (HRTEM) coupled with neutron powder diffraction (NPD) and synchrotron X-ray diffraction (SXRPD) at room temperature. Moreover, bearing in mind that seven lithium atoms were reversibly deintercalated from the latter phase [20], we also studied the product phase $Li_5Mo_5O_{17}$ using HRTEM. We will illustrate the great flexibility of the $[Mo_5O_{17}]_\infty$ ribbons to accommodate lithium cations and the variation of molybdenum valency.

2. Experimental

The parent phase $Li_4Mo_5O_{17}$ was first prepared via sol gel method already described [20]. The electrochemistry characterization of $Li_4Mo_5O_{17}$ was performed in Swagelok cells. The negative electrode was metallic Li (Aldrich, 99.9%), LP30 from Merck (1 M $LiPF_6$ in an ethylene carbonate (EC)/dimethyl carbonate (DMC) 1:1 w/w Selectipur) was used as electrolyte and the positive electrode was constituted of approximately 10 mg

* Corresponding author. Fax: +33 2 31 95 16 00.
E-mail address: valerie.pralong@ensicaen.fr (V. Pralong).

0022-4596/$ - see front matter © 2011 Elsevier Inc. All rights reserved.
doi:10.1016/j.jssc.2011.02.001

mixture of the active material with 30% carbon (acetylene black). The electrochemical cells were cycled on a VMP II potentiostat/galvanostat (Biologic SA, Claix, France) at room temperature. Potentiostatic intermittent titration technique (PITT) measurements were conducted using potential steps of 10 mV limited by a minimum current equivalent to a C/100 galvanostatic rate. This technique was first proposed by Thompson et al. [22,23]. Recording the chronoamperometric responses of the system during every potential level gives access to the evolution of the kinetics for each redox level. This enables us to distinguish between a single-phase solid solution domain in which the kinetics is most often governed by diffusion laws, and a two phase domain in which the kinetics is usually governed by the mobility of the interface between the two phases [24–28], similar to what is observed for nucleation and growth processes [29–31]. Note that despite the low rate used for the electrochemical analysis, only 6 lithiums could be inserted due to the large particle size. Thus, for the HRTEM and neutron study, the end members were prepared by chemical reduction and the lithium content was confirmed by AAS analysis.

The chemical reduction of the parent phase $Li_4Mo_5O_{17}$ lead to $Li_{12}Mo_5O_{17}$ (Eq. (1), 3 days, room temperature, stirring):

$$Li_4Mo_5O_{17} + n\text{Bu-Li (10 mL, 2.5 M)} + \text{hexane} \rightarrow Li_{12}Mo_5O_{17} + \text{hexane} + \text{butane} \quad (1)$$

At that point, it is important to mention that on the electrochemical curve, no major activity is observed between 2.0 and 1.0 V.

The chemical oxidation of the chemically reduced phase $Li_{12}Mo_5O_{17}$ leads to $Li_5Mo_5O_{17}$ as follows (Eq. (2)):

$$Li_{12}Mo_5O_{17} + 7NO_2BF_4 \rightarrow Li_5Mo_5O_{17} + 7LiBF_4 + 7NO_2 \quad (2)$$

The XRD pattern of the end members $Li_{12}Mo_5O_{17}$ and $Li_5Mo_5O_{17}$ prepared from either electrochemistry or chemistry are really similar. The lithium content was determined by atomic absorption spectroscopy with a Varian Spectra AA-20 instrument. Note that the samples were dissolved in a mixture of H_2O_2/NH_3.

Neutron diffraction experiment was carried out at HRPT diffractometer (PSI, Villigen) with a wavelength of 1.886 Å. The synchrotron X-ray diffraction patterns were registered on the MS X04AS beam line (PSI, Villigen) using a wavelength of 0.6522 Å between 1° and 60° with a step 0.003757° (2θ).

The electron diffraction (ED) and HRTEM study has been carried out on crushed samples, dissolved in butanol and deposited on a holey carbon grid. The microscope was a JEOL 4000 EX operated at 400 kV and having 0.17 nm point resolution. Simulation of the HRTEM images was performed using the Mac Tempas and Crystal Kit software.

3. Results and discussion

3.1. The ordered rock salt structure of $Li_{12}Mo_5O_{17}$

The electron diffraction study of $Li_{12}Mo_5O_{17}$ reveals two types of the structures with somehow different parameters. The [010] and [100] ED patterns of the first one (Type I) shown in Fig. 1a are in agreement with the previously reported [20] triclinic $P-1$ structure with cell parameters. $a\sim6.8$ Å, $b\sim9.5$ Å, $c\sim10.8$ Å, $\alpha\sim73.1°$, $\beta\sim89°$ and $\gamma\sim69.8°$. The second structure (Type II) exhibits ED patterns along the main [010] and the [100] zone axis similar to Type I, but weak superstructure reflections along the [001] direction suggest a doubling of the ***c***-parameter, i.e. $c\sim21.6$ Å (Fig. 1b). In order to confirm the Type I structure of $Li_{12}Mo_5O_{17}$ reported previously [20] and to clarify the nature of the *c*-axis doubling in the Type II structure, a HRTEM study has been performed. The results are shown in Fig. 2.

The [010] HRTEM image of the Type I phase (Fig. 2a) shows rows of brighter dots running along the *a*-axis and spaced by ~11 Å in the *c*-direction, which alternate with 5-dot strips of less bright spots. Bearing in mind the previous structural analysis and image simulation, Mo atoms correspond to black dots and the 5-dot strips of less bright spots represent the stacking of the $[Mo_5O_{17}]_\infty$ ribbons, which are running along [−373] and are five MoO_6 octahedra thick. The rows of brighter dots correspond to

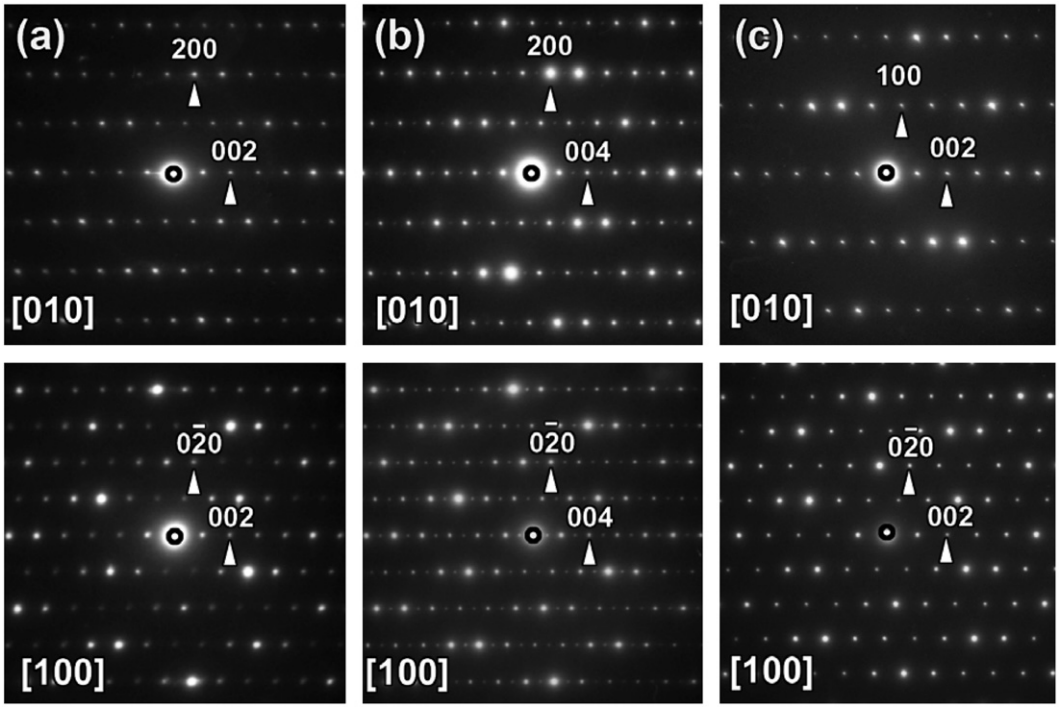

Fig. 1. ED patterns taken along two [100] and [010] relevant zones for (a) Type I and (b) Type II $Li_{12}Mo_5O_{17}$ structures and (c) $Li_5Mo_5O_{17}$.

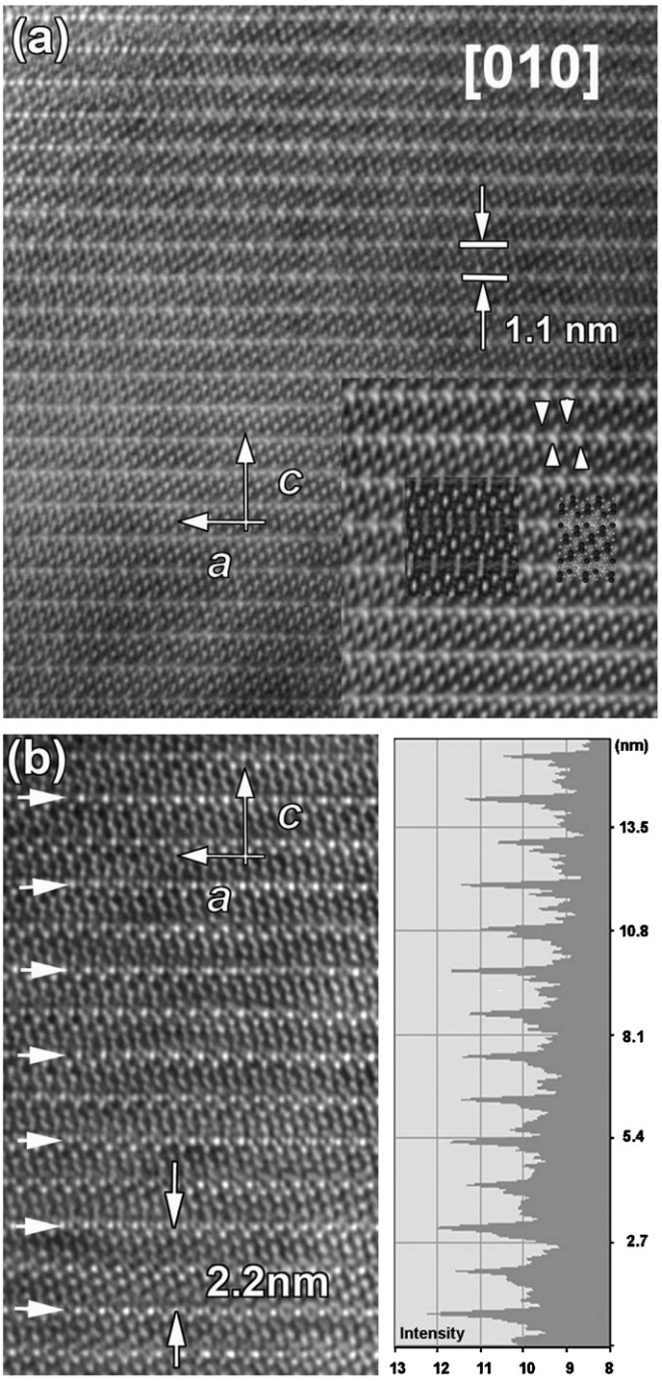

Fig. 2. (a) [010] HRTEM image of Type I $Li_5Mo_5O_{17}$ structure. Enlargement and simulated images based on corrected model (see Table 1) together with atomic overlay model are given as inset (Dt = −20 nm, t = 10 nm). (b) [010] HRTEM image of Type II $Li_{12}Mo_5O_{17}$ structure showing doubling of *c*-parameter (marked by white arrows). Intensity plot profile given below demonstrates clear intensity modulation along the *c*-axis one out of two layers.

the adjusting plane between these ribbons which should be occupied by lithium (see enlargement in Fig. 2a). Attempts to simulate this image, based on the atomic positions previously determined from XRPD data do not lead to satisfactory results. In particular, on this image one observes that within the bright rows, one very bright dot alternates with a less bright dot (see arrow in Fig. 2a), whereas the simulations based on the previous XRPD (not shown in the figure) results implies that all bright dots of these rows should have an equal intensity. This point will be further explained, after having described the neutron diffraction study.

The [010] HRTEM image of Type II crystals basically exhibit a contrast similar to Type I crystals (Fig. 2b). However, consistent with the ED pattern in Fig. 1b, the HRTEM image shows a clear doubling of the periodicity in the ribbon's "adjusting plane" (see overlay model in the enlargement of Fig. 2a). It should be noticed that HRTEM measurements of this material are far from trivial because of its instability under the electron beam inside a microscope. We found out that the Type I crystals are more stable under the e-beam, whereas for the doubling to the *c*-axis in Type II crystals disappears very fast, leading to a Type I appearance. Note therefore the phase with the superstructure could not be detected from neutron study, showing that in any case it is in minority.

The SXRPD data registered on the SLS diffractometer MSXO4SA confirm the triclinic $P-1$ space group and the cell parameters ($a=6.554(1)$ Å, $b=8.849(1)$ Å, $c=11.606(2)$ Å, $\alpha=77.54(1)^\circ$, $\beta=96.34(1)^\circ$, $\gamma=72.04(1)^\circ$). However the full profile refinement shows that the Bragg reflections are anisotropic, which render the Rietveld refinement [32] very difficult, and consequently prevent accurate positions to be obtained. Therefore, the Rietveld refinement, was conducted with NPD data (Fig. 3), collected on the SINQ diffractometer HRPT. Soft constraints were used during the refinement, which were progressively released. The refinement of molybdenum, oxygen and lithium atom positions with Fullprof [23] successively led to the following fit values: $R_{WP}=5.36$, $R_B=7.6\%$ and $\chi^2=7.35$. The atomic coordinates (Table 1) are close to those observed in the previous XRPD data. This result was of course expected for the Mo and O positions but allows a better accuracy for the lighter oxygen atom. More important, the atomic positions of the lithium cations are close to those predicted previously from BVS calculations.

A structural view of $Li_{12}Mo_5O_{17}$ along a direction close to the [−373] direction (Fig. 4a) of the triclinic cell shows that the infinite $[Mo_5O_{17}]_\infty$ ribbons running along that direction exhibit a similar geometry as the one previously observed for $Li_4Mo_5O_{17}$. An important point is the regular geometry of the MoO_6 octahedra of $Li_{12}Mo_5O_{17}$ compared to the one in $Li_4Mo_5O_{17}$. The interatomic Mo–O distances (Table 2) indeed show values comprised between 1.935 and 2.11 Å for the Mo1, Mo3 and Mo5 octahedra, whereas the Mo(2) and Mo(4) octahedra are slightly more distorted with distances ranging from 1.96 to 2.14 Å and from 1.90 to 2.25 Å, respectively. This much higher symmetry of the MoO_6 octahedra, compared to $Li_4Mo_5O_{17}$, where the Mo–O distances are comprised between 1.70 and 2.49 Å, is explained by

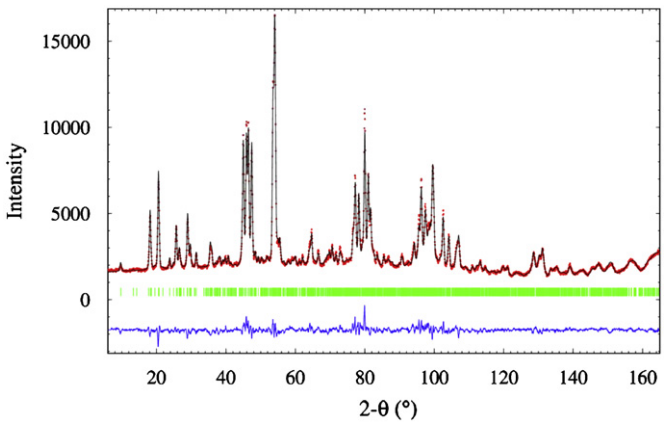

Fig. 3. Rietveld refinement plot of $Li_5Mo_5O_{17}$: observed (dots), calculated (line) and difference (bottom line) neutron diffraction pattern. Allowed Bragg reflections (vertical bars) are marked.

Table 1
Atomic coordinates for $Li_{12}Mo_5O_{17}$.

Atom	Wyck.	*x/a*	*y/b*	*z/c*	*U* (Å²)
Mo1	2*i*	0.170(2)	0.7873(16)	0.6970(11)	0.0127(6)
Mo2	2*i*	0.229(2)	0.4713(17)	0.8317(12)	0.0127(6)
Mo3	2*i*	0.243(2)	0.9308(19)	0.3513(13)	0.0127(6)
Mo4	2*i*	0.6679(20)	0.1767(14)	0.8966(11)	0.0127(6)
Mo5	2*i*	0.709(2)	0.3423(17)	0.5262(13)	0.0127(6)
Li1	2*i*	0.545(3)	0.829(3)	0.5778(18)	0.0268(14)
Li2	2*i*	0.926(3)	0.585(3)	0.5993(18)	0.0268(14)
Li3	2*i*	0.003(3)	0.258(3)	0.7572(18)	0.0268(14)
Li4	2*i*	0.400(3)	0.999(3)	0.7737(18)	0.0268(14)
Li5	2*i*	0.291(3)	0.123(3)	0.9930(18)	0.0268(14)
Li6	2*i*	0.124(3)	0.108(3)	0.5421(18)	0.0268(14)
Li7	2*i*	0.334(3)	0.317(2)	0.6346(18)	0.0268(14)
Li8	2*i*	0.596(3)	0.518(3)	0.7217(18)	0.0268(14)
Li9	2*i*	0.806(3)	0.737(2)	0.8142(18)	0.0268(14)
Li10	2*i*	0.522(3)	0.350(2)	0.0711(18)	0.0268(14)
Li11	2*i*	0.941(3)	0.066(3)	0.1050(18)	0.0268(14)
Li12	2*i*	0.881(3)	0.400(3)	0.9574(18)	0.0268(14)
O1	2*i*	0.478(2)	0.7512(18)	0.7522(13)	0.0122(3)
O2	2*i*	0.141(2)	0.7015(19)	0.8653(13)	0.0122(3)
O3	2*i*	0.256(2)	0.5621(18)	0.6506(14)	0.0122(3)
O4	2*i*	0.853(2)	0.8254(18)	0.6395(13)	0.0122(3)
O5	2*i*	0.207(3)	0.8715(19)	0.5252(13)	0.0122(3)
O6	2*i*	0.081(3)	0.0197(18)	0.7198(13)	0.0122(3)
O7	2*i*	0.205(3)	0.3723(19)	1.0111(14)	0.0122(3)
O8	2*i*	0.568(3)	0.4220(19)	0.8985(14)	0.0122(3)
O9	2*i*	0.920(2)	0.5015(18)	0.7814(13)	0.0122(3)
O10	2*i*	0.333(3)	0.2267(19)	0.8175(13)	0.0122(3)
O11	2*i*	0.546(3)	0.9222(18)	0.3957(14)	0.0122(3)
O12	2*i*	0.331(2)	0.7228(18)	0.2988(13)	0.0122(3)
O13	2*i*	0.271(3)	0.0180(18)	0.1731(13)	0.0122(3)
O14	2*i*	0.969(2)	0.1638(19)	0.9331(14)	0.0122(3)
O15	2*i*	0.613(2)	0.1120(17)	0.0547(13)	0.0122(3)
O16	2*i*	0.005(3)	0.3357(19)	0.5730(14)	0.0122(3)
O17	2*i*	0.390(2)	0.4131(18)	0.4613(13)	0.0122(3)

the fact that molybdenum exhibits a smaller valence Mo(V)–Mo(IV) in $Li_{12}Mo_5O_{17}$ and also most probably a tendency to electronic delocalization within the $[Mo_5O_{17}]_\infty$ ribbons, whereas in $Li_4Mo_5O_{17}$, hexavalent molybdenum exhibits a d° configuration favorable to distortion. Note that the average Mo–O distance in the MoO_6 octahedra, ranging from 2.02 to 2.09 Å is in agreement with the ionic radii of Mo(V)/Mo(IV) mixed valence according to Shannon and Prewitt [33]. Moreover the Mo–Mo distances within the octahedral ribbons are generally close to 3 Å (Table 2) as often observed for edge-sharing octahedra. Nevertheless Mo1–Mo2 distances are very short (2.74 Å) and Mo3–Mo5 distances are exceptionally short (2.43 Å), suggesting that the electronic delocalization between these two latter species might appear through direct overlapping of the 4*d* orbitals of molybdenum.

The representation of the structure of this phase in terms of both Li and Mo polyhedra, along the same [−373] direction (Fig. 4b) clearly shows that both LiO_6 and MoO_6 octahedra form an ordered rock salt structure. It is quite remarkable that the LiO_6 octahedra form, in this description, the main framework, hosting the octahedral ribbons of molybdenum. The interatomic Li–O distances (Table 2), ranging from 2.04 to 2.20 Å, show that the 12 independent Li^+ cations exhibit an almost regular octahedral coordination. Most of the Li^+ cations exhibit an average Li–O distance ranging from 2.09 to 2.13 Å (Li1–Li9). Such a value is close to the theoretical prediction according to Shannon and Prewitt. Remarkably the cations Li10–Li12, show smaller average Li–O distances, ranging from 2.06 to 2.07 Å. Moreover, the coordination of these three cations located at the junction of three ribbons is the most regular.

At this point, let us re-evaluate the simulation of the [010] HRTEM image, using the atomic coordinates determined from NPD data. The comparison of the experimental and simulated images (inset Fig. 2a) clearly shows that the structure determined

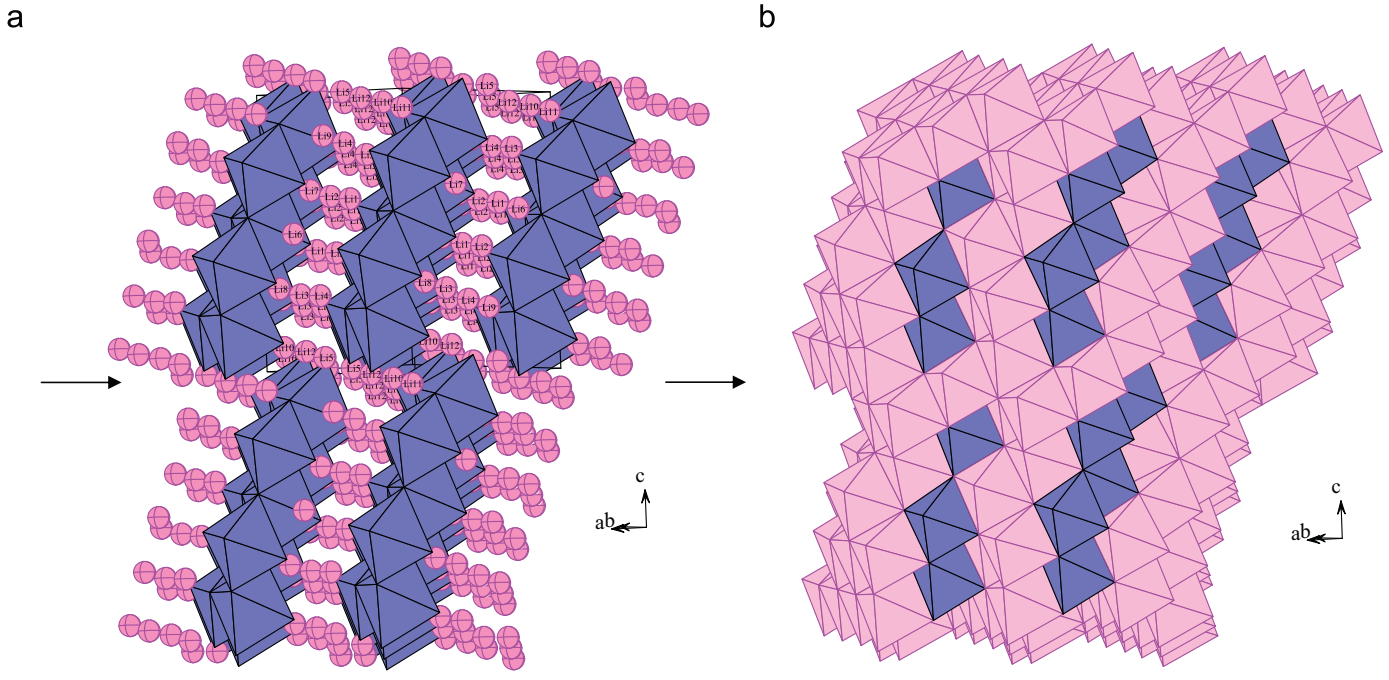

Fig. 4. $Li_5Mo_5O_{17}$. View of the structure (a) close to the [−373] direction of the triclinic cell. Observe the infinite octahedral ribbons $[Mo_5O_{17}]_\infty$ of edge sharing octahedra, with a similar arrangement to that obtained for $Li_5Mo_5O_{17}$. The large sphere correspond to the Li+ cations intercalated between the infinite octahedral $[Mo_5O_{17}]_\infty$ ribbons (b) close to [−373] direction of the triclinic cell, showing both LiO_6 and MoO_6 octahedra forming the ordered rock salt structure. The LiO_6 octahedra (light color) appear as the main framework, hosting the ribbons of MoO_6 octahedra (dark color) (for interpretation of the references to color in this figure legend, the reader is referred to the web version of this article).

Table 2
$Li_{12}Mo_5O_{17}$: interatomic distances.

Mo1–O	**Mo2–O**	**Mo3–O**	**Mo4–O**	**Mo5–O**
1.953				
	1.962	1.969	1.909	1.935
1.990				
	2.074	2.000	1.934	1.993
2.010				
	2.108	2.032	2.008	2.038
2.041				
	2.121	2.065	2.071	2.057
2.042				
	2.130	2.083	2.153	2.102
2.101				
	2.145	2.095	2.252	2.110
〈**2.023 Å**〉	〈**2.090**〉	〈**2.032**〉	〈**2.054**〉	〈**2.039**〉
Mo1–Mo2=2.779				
Mo1–Mo3=2.959				
Mo1–Mo5=3.135				
Mo2–Mo4=3.112				
Mo3–Mo5=2.431				
Mo3–Mo4=3.276				
Mo5–Mo5=3.138				

Li1–O	**Li2–O**	**Li3–O**	**Li4–O**	**Li5–O**
2.054				
	2.092	2.096	2.045	2.041
2.098				
	2.106	2.103	2.047	2.118
2.124				
	2.113	2.111	2.055	2.131
2.132				
	2.118	2.142	2.111	2.132
2.196				
	2.196	2.157	2.126	2.165
2.208				
	2.202	2.162	2.169	2.189
〈**2.135**〉	〈**2.138**〉	〈**2.129**〉	〈**2.092**〉	〈**2.129**〉

Li6–O	**Li7–O**	**Li8–O**	**Li9–O**	**Li10–O**	**Li11–O**	**Li12–O**
2.049			2.069			2.025
	2.102	2.091		2.040	2.049	
2.053			2.102			2.043
	2.124	2.096		2.051	2.049	
2.118			2.111			2.068
	2.138	2.100		2.052	2.051	
2.124			2.116			2.080
	2.139	2.107		2.062	2.075	
2.161			2.147			2.100
	2.140	2.110		2.053	2.094	
2.098			2.147			2.124
	2.126	2.172		2.122	2.096	
〈**2.101**〉	〈**2.128**〉	〈**2.113**〉	〈**2.111**〉	〈**2.063**〉	〈**2.069**〉	〈**2.073**〉

from the NPD refinement renders perfectly account of the particular contrast. The alternation of bright dots and less bright dots along *a* is clearly seen on the enlargement (inset Fig. 2a). It corresponds in fact to small displacements of the Mo and O atoms which are located on both sides of the "Mo_5O_{17}" ribbons as it is shown in the model in Fig. 8b (see arrows), with respect to the positions deduced from the XRPD calculations (Fig. 8a).

3.2. HRTEM of $Li_5Mo_5O_{17}$: mechanism of Li insertion/deinsertion

In our previous study, we observed that the Li electrochemical intercalation in $Li_4Mo_5O_{17}$ proceeds through two biphasic processes [20], i.e. there is no solid solution between $Li_4Mo_5O_{17}$ and $Li_{12}Mo_5O_{17}$ (see Fig. 5). Curiously, during the electrochemical deintercalation of $Li_{12}Mo_5O_{17}$, a new phase $Li_5Mo_5O_{17}$, was obtained at 3.0 V (see Fig. 5). Unfortunately, we were unable to produce enough of this oxide for an NPD study. Nevertheless, the $Li_5Mo_5O_{17}$ phase was found quite stable and well crystallized. In order to understand the mechanism of Li intercalation–deintercalation in the $Li_xMo_5O_{17}$ system, we have revisited the structural behavior of the deintercalated $Li_5Mo_5O_{17}$ phase, using HRTEM.

The ED study of $Li_5Mo_5O_{17}$, confirms its triclinic symmetry with space group $P-1$, as previously observed [20], and evident from its [100] and [010] ED patterns (Fig. 1c). The following cell parameters, $a=6.761$ Å, $b=9.508$ Å, $c=10.829$ Å, $\alpha=72.87^\circ$, $\beta=88.59^\circ$, $\gamma=69.71^\circ$, similar to those of $Li_4Mo_5O_{17}$, are confirmed, in agreement with the previous XRPD investigation. HRTEM shows that its structure is very similar to that of $Li_4Mo_5O_{17}$. This feature is illustrated by the [110] image of this oxide (Fig. 6). According to the image simulation based on the $Li_4Mo_5O_{17}$

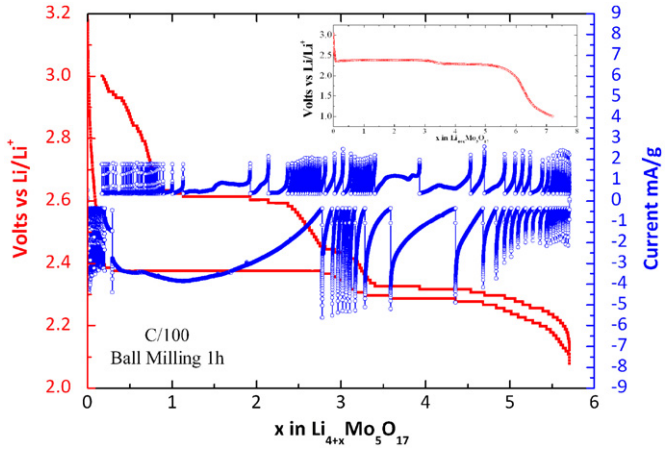

Fig. 5. Potentiometric titration curve (PITT) during the first cycle of $Li_5Mo_5O_{17}$ in the range 3.0–2.0 V vs. Li/Li^+ limitation of the 10 mV potential step in duration of 1 h and current limitation equivalent to a galvanic current $I_{limit}=I_{C/100}$. Inset: galvanostatic first discharge until 1.0 V vs. Li+/Li.

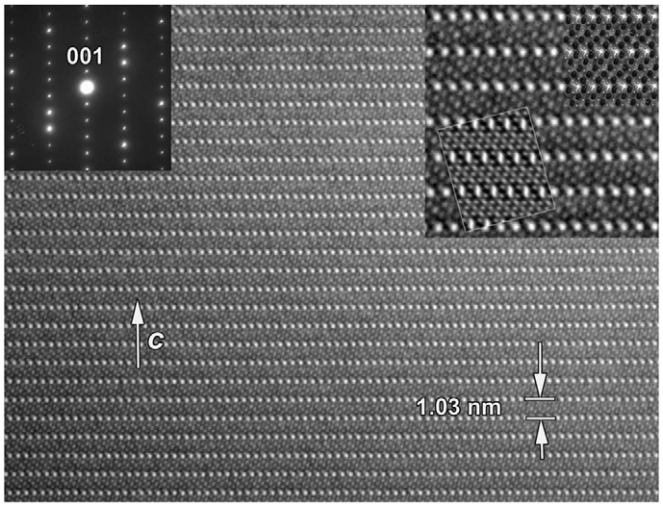

Fig. 6. [010] HRTEM image of $Li_5Mo_5O_{17}$ structure and corresponding ED pattern. Image simulation based on of $Li_5Mo_5O_{17}$ structure given as inset in enlargement image together with overlay structural model (Mo – blue and Li – yellow atoms) of $Li_5Mo_5O_{17}$ (for interpretation of the references to color in this figure legend, the reader is referred to the web version of this article).

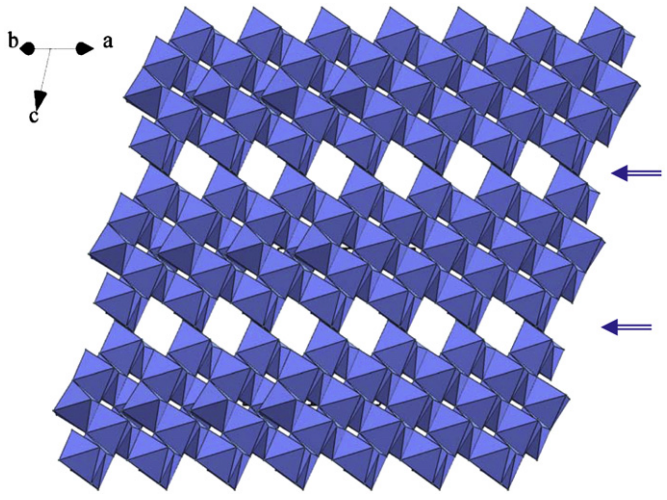

Fig. 7. 〈110〉 Structural view of $Li_5Mo_5O_{17}$.

structure, previously obtained from single crystal X ray diffraction data [16], the rows of large brighter dots running along [110] correspond to zones of lower electron density, i.e. to the zones located at the border of the strips built up of ribbons of MoO_6 octahedra (see arrows in Fig. 7), whereas the much smaller and less bright spots correspond to the space between the octahedral ribbons. At first sight, this [110] HRTEM image appears to be very similar to the one of $Li_4Mo_5O_{17}$ and the calculated image (see inset in Fig. 6) fits rather well the experimental one. Nevertheless, it differs from the latter by the shape of the brighter dots which are oval instead of perfectly round. Bearing in mind that 20% additional lithium should be inserted into this oxide with respect to $Li_4Mo_5O_{17}$, we have to locally adapt the Li coordination, possibly at the boundary between the strips of ribbons (horizontal arrows of Fig. 7). We therefore have displaced the Mo atoms located at the boundary of the strips by very small distances; less than 0.2 Å (see curved arrows in Fig. 7), so that we obtain a more symmetric environment for Li (Fig. 8c). For such a structural model, the simulated HRTEM image shows brighter dots that are much more circular and perfectly fits with the experimental one.

Because of the limited resolution and the radiation sensitivity of the sample inside the microscope, we are unable to obtain quantitative data about the displacement and/or distortion of the MoO_6 octhahedra in the structure. However, our results clearly illustrate the similarity of the $Li_5Mo_5O_{17}$ and the $Li_4Mo_5O_{17}$ structures. The differences being in a different coordination of lithium in both structures, resulting from a slight change of the

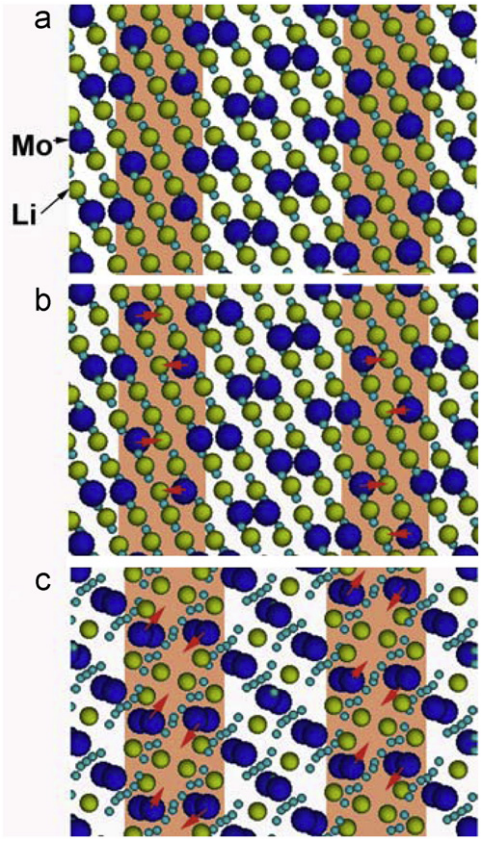

Fig. 8. Structural model of $Li_5Mo_5O_{17}$ determine by XRD in [20] – (a) and determine by combination of HRTEM and NPD in present work – (b) viewed along the [010] direction, (c) – structural model of $Li_5Mo_5O_{17}$ viewed along the [110] zone axis. The displacements of Mo atoms (blue) leading to best fitting experimental and simulated HRTEM images are shown by red arrows (for interpretation of the references to color in this figure legend, the reader is referred to the web version of this article).

geometry of the MoO_6 octahedra located at the border of the octahedral strips. The difficulty to completely deintercalate lithium from "Li_5" to "Li_4" can be explained by the fact that in $Li_{12}Mo_5O_{17}$ the Li^+ cations located at the border of the octahedral strips (Li10–Li11–Li12) exhibit shorter Li–O distances and are more strongly linked and may rearrange differently with the surrounding oxygen atoms during deintercalation. In a similar way, it can be understood that the process of Li intercalation in $Li_4Mo_5O_{17}$, requires specific conditions for the intercalation of the last two or three Li^+ cations, since the space left at the junction between the strips is smaller, beyond the composition $Li_8Mo_5O_{17}$, introducing strains.

4. Conclusion

In this study, we have clearly illustrated the ability of a ribbon structure $Li_4Mo_5O_{17}$ to transform topotactically into an ordered rock salt type structure $Li_{12}Mo_5O_{17}$, and we have explained the reversibility of the process of intercalation–deintercalation limited to the member $Li_5Mo_5O_{17}$. From the viewpoint of lithium intercalation, the $Li_xMo_5O_{17}$ system appears as exceptional compared to many other oxides, because of its capacity to intercalate up to 1.6 Li per Mo, and to contain 2.4 Li per Mo, whereas most of other transition metal oxide can only intercalate a maximum of 1 Li per transition element. Such a property is due to the concomitant existence of two important factors: the molybdenum valence, which covers a wide range from Mo^{+6} to Mo^{+4} and the peculiar geometry of this structure which consists of ribbons of MoO_6 octahedra with a configuration, precursor of a rock salt structure. In this respect, the intercalation/deintercalation properties of these phases are directly related to the exceptional assemblage of the $[Mo_5O_{17}]_\infty$ ribbons forming strips which are five MoO_6 octahedra thick, so that we should distinguish the Li^+ cations inserted within the strips between the ribbons, and those inserted at the border of the strips between them. It is this exceptional structure, which allows a great flexibility of the geometry of the $[Mo_5O_{17}]_\infty$ ribbons and a particular role of the interspaces between the successive strips for lithium intercalation/deintercalation. It is on this basis, that other transition metal oxides with a ribbon structure should be investigated or synthesized, in view of discovering new oxides for Li ion battery applications.

The combination of electron diffraction and HRTEM allowed identifying a new $Li_{12}Mo_5O_{17}$ structure with double *c*-parameter.

Acknowledgments

This work was based on the results obtained at the Swiss spallation neutron source SINQ, Pauls Scherrer Institut, Switzerland. The authors are grateful to Dr. D. Sheptyakov for technical help for the neutron diffraction and fruitful scientific discussion. We want also to thank Dr. S. Malo for fruitful discussion regarding TEM analysis. We gratefully acknowledge the CNRS and the Minister of Education and Research for financial support through their Research, Strategic, and Scholarship programs, and the European Union for support through the network of excellence Novelox. The authors acknowledge support from the European Union under the Framework 6 program under a contract from an Integrated Infrastructure Initiative (Reference 026019 ESTEEM).

References

[1] M.S. Whittingham, Chem. Rev. 104 (2004) 4271.
[2] B.L. Ellis, K.T. Lee, L.F. Nazar, Chem. Mater. 22 (2010) 691.
[3] M. Armand, J.M. Tarascon, Nature 451 (2008) 652.
[4] T. Ohzuku, R.J. Brodd, J. Power Sources 174 (2) (2007) 449–456.
[5] J.B. Goodenough, Y. Kim, Chem. Mater. 22 (2010) 587–603.
[6] T. Ohzuku, R.J. Brodd, J. Power Sources 174 (2007) 449–456.
[7] A. Martinez-de-la-Cruz, I. Suarez-Ramirez, J. Power Sources 133 (2004) 268.
[8] J. Song, X. Wang, X. Wang, X. Ni, H. Zheng, Z. Zhang, M. Ji, T. Shen, Mater. Res. Bull. 40 (2005) 1751.
[9] F. Leroux, L.F. Nazar, Solid State Ionics 133 (2000) 37.
[10] S.S. Kim, S. Ogura, H. Ikuta, Y. Uchimoto, M. Wakihara, Solid State Ionics 146 (2002) 249.
[11] H. Kobayashi, M. Tabuchi, M. Shikano, Y. Nishimura, H. Kageyama, T. Ishida, H. Nakamura, Y. Kurioka, R. Kanno, J. Power Sources 81–82 (1999) 524.
[12] R. Schollhorn, R. Kuhlmann, J.O. Besenhard, Mater. Res. Bull. 11 (1976) 83.
[13] C.K. Huang, S. Crouch-Baker, R.A. Huggins, J. Electrochem. Soc. 135 (1988) 408.
[14] T. Tsumara, M. Inagaki, Solid State Ionics 104 (1997) 183.
[15] A.C. James, J.B. Goodenough, J. Solid State Chem. 76 (1988) 87.
[16] M. Wiesman, H. Heitzel, I. Svoboda, H. Fuess, Z. Kristallogr. 212 (1997) 795.
[17] W.S. Brower, H.S. Parker, R.S. Roth, J.L. Waring, J. Cryst. Growth 16 (1972) 115.
[18] B.M. Gatehouse, B.M. Miskin, J. Solid State Chem. 9 (1974) 247; B.M. Gatehouse, B.M. Miskin, J. Solid State Chem. 15 (1975) 274.
[19] J.P. Smith, P.C. Stair, K.R. Poppelmeier, Cryst. Growth Des. 7 (2007) 521.
[20] N. Pop, V. Pralong, V. Caignaert, J.F. Colin, S. Malo, G. Van Tendeloo, B. Raveau, Chem. Mater. 21 (2009) 3242.
[21] V. Pralong, Prog. Solid State Chem. 37 (2009) 262.
[22] A.H. Thompson, J. Electrochem. Soc. 126 (1979) 603.
[23] A.H. Thompson, Rev. Sci. Instrum. 54 (1983) 229.
[24] S.-I. Pyun, Y.-G. Yoon, Mol. Cryst. Liq. Cryst. 123 (1998) 311.
[25] N. SacEpee, M.R. Palacin, B. Beaudouin, A. Delahaye-Vidal, T. Jamin, Y. Chabre, J.-M. Tarascon, J. Electrochem. Soc. 144 (1997) 3896.
[26] V. Pralong, A. Delahaye-Vidal, Y. Chabre, J.M. Tarascon, J. Solid State Chem. 162 (2001) 270.
[27] Y. Chabre, Physics of Intercalation II, NATO ASI Ser. B 305 (1993) 181.
[28] H.-C. Shin, S.I. Pyun, Electrochim. Acta 44 (1999) 2235.
[29] J. Philibert, Atom Movement, Diffusion and Mass Transport in Solid, Les Editions de Physique, Les Ulis, 1991.
[30] B.R. Sharifker, G.J. Hills, Electrochim. Acta 28 (1983) 879.
[31] Southampton Electrochemistry Group, Instrumental Methods in Electrochemistry, Ellis Horwood Series in Physical Chemistry,1985.
[32] J. Rodriguez-Carvajal, Physica B 192 (1993) 55.
[33] R.D. Shannon, C.T. Prewitt, Acta Crystallogr. B 25 (1969) 925–946.